

Anomalous proximity effect of a spin-singlet superconductor with a spin-orbit interactionJaechul Lee ¹, Satoshi Ikegaya ², and Yasuhiro Asano ¹¹*Department of Applied Physics, Hokkaido University, Sapporo 060-8628, Japan*²*Institute for Advanced Research, Nagoya University, Nagoya 464-8601, Japan*

(Received 28 January 2025; revised 23 April 2025; accepted 24 April 2025; published 13 May 2025)

The anomalous proximity effect of a spin-triplet p -wave superconductor has been known as a part of Majorana physics, and is explained by the penetration of zero-energy states from a surface of a superconductor to a dirty normal metal. We demonstrate that a spin-singlet d -wave superconductor without any surface zero-energy states exhibits the anomalous proximity effect in the presence of a specific spin-orbit interaction. The results show the quantization of the zero-bias conductance in a dirty normal-metal/superconductor junction. We also discuss a relation between our findings and results in an experiment on a $\text{CoSi}_2/\text{TiSi}_2$ junction.

DOI: [10.1103/PhysRevB.111.174516](https://doi.org/10.1103/PhysRevB.111.174516)**I. INTRODUCTION**

When a superconductor (SC) is attached to a normal metal, Cooper pairs penetrate from the SC into the normal metal and modify its electromagnetic and thermal properties. This phenomenon, known as the proximity effect, exhibits distinct behavior depending on the symmetry of the pair potential. Specifically, the proximity effect of a spin-triplet p -wave SC indicates remarkable transport phenomena such as the quantization of zero-bias conductance in a dirty normal-metal/superconductor (DN/SC) junction [1,2] and the fractional current-phase relationship of a Josephson currents in a SC/DN/SC junction [3,4]. These unusual phenomena are referred to as the anomalous proximity effect (APE).

The APE is a result of the interplay between two interference effects: the proximity effect in a DN attached to a SC and the formation of Andreev bound states at the surface of a SC. The presence or absence of the proximity in a DN depends sensitively on the symmetry of the pair potential [5]. To host Andreev bound states at the surface of a SC, it is necessary for the pair potential to change its sign on the Fermi surface [6–9]. Symmetry analysis in the early stages of study suggested that the APE is a phenomenon unique to spin-triplet SCs [4]. In addition to the conductance quantization in a DN/SC junction, the APE causes the zero-bias anomaly of the conductance spectra in a T-shaped junction [10], and unusual surface impedance [11]. Unfortunately, it would be very difficult to observe the APEs in experiments because spin-triplet SCs are very rare. A topological material based compound, $\text{Cu}_x\text{Bi}_2\text{Se}_3$, and several uranium compounds such as UPt_3 , UBe_{13} , UGe_2 , and UTe_2 are candidates of the spin-triplet SC [12–18]. However, spin-triplet superconductivity in these materials is still under debate.

The fabrication of artificial spin-triplet SCs is an important issue these days to realize quantum computation by applying non-Abelian statistics of Majorana fermions [19–24]. The APE is a part of Majorana physics because Majorana zero modes are a special case of the Andreev bound states at the surface of a spin-triplet SC [23]. These theoretical studies have suggested that spin-orbit interactions (SOIs) enable the

realization of spin-triplet superconductivity in a spin-singlet SC. Moreover, a theory shows that a nonzero integer number \mathcal{N}_{ZES} , mathematically known as an Atiyah-Singer index, represents exactly the quantized value of the zero-bias conductance in a DN/SC junction [25,26]. According to their argument, \mathcal{N}_{ZES} represents the number of zero-energy states that penetrate from a surface of SC into a DN and form the resonant transmission channels. This conclusion leads us to infer that spin-triplet superconductivity is only a sufficient condition for $\mathcal{N}_{\text{ZES}} \neq 0$. Two of authors looked for necessary conditions for the Bogoliubov–de Gennes (BdG) Hamiltonian that provide a nonzero \mathcal{N}_{ZES} [27]. We found that several Hamiltonians breaking time-reversal symmetry lead to a nonzero index, and they describe the artificial SCs hosting Majorana zero modes [27–29]. In addition, we also found that a Hamiltonian for a spin-singlet d_{xy} -wave SC with a specialized SOI gives a nonzero index [30,31]. It has been well established that a d_{xy} -wave SC without SOIs hosts highly degenerate zero-energy states at its clean surface parallel to the y direction [6–9]. But in the absence of SOIs, $\mathcal{N}_{\text{ZES}} = 0$ holds true, which means that zero-energy states are fragile under impurity scatterings. A SOI transforms such fragile zero-energy states to robust zero-energy states [30,31].

In 2021, an experiment observed a clear signal of APE [32]. The conductance spectra in a T-shaped junction connecting to CoSi_2 grown on a Si substrate show the zero-bias anomaly, which is a typical phenomenon of the APE [10]. Their transport measurement indicates strong SOIs near the interface between a thin CoSi_2 single crystal and a Si substrate [33,34]. However, spin-singlet s -wave superconductivity has been well established in bulk CoSi_2 [35,36]. Unlike a d_{xy} -wave SC, the zero-energy states are absent at the junction interface. At present, it is not clear if SOIs can cause the APE in a junction that consists a spin-singlet SC without any surface Andreev bound states. We discuss this issue in the present paper.

In this paper, we theoretically study the differential conductance in a DN/SC junction as shown in Fig. 1. We assume the spin-singlet s -wave and spin-singlet $d_{x^2-y^2}$ -wave pair potentials in a SC. In the absence of SOIs, the Andreev bound

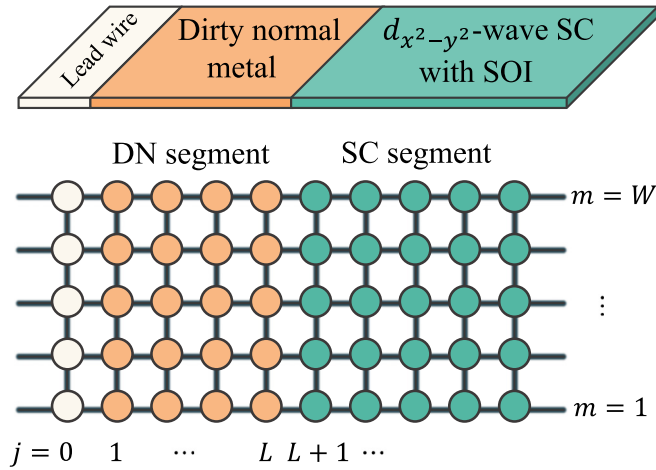


FIG. 1. Schematic figure of a two-dimensional dirty normal-metal/SC junction. We consider spin-singlet pair potentials (s wave or $d_{x^2-y^2}$ wave) and three types of spin-orbit interactions in a SC. We also introduce nonmagnetic random impurities in a normal metal.

states are absent at a junction interface. We introduce three types of SOIs in a SC and the nonmagnetic random impurity potential in a DN. The conductance is calculated based on the Blonder-Tinkham-Klapwijk formula and the transport coefficients are obtained by using the recursive Green's function method. A $d_{x^2-y^2}$ -wave SC with a persistent spin-helix type SOI causes the APE. Unfortunately, an s -wave SC does not exhibit the APE with any types of SOIs.

This paper is organized as follows. We explain our theoretical model in Sec. II. The results of the differential conductance are presented in Sec. III. We explain why a persistent spin-helix type SOI is necessary for the APE and why an s -wave SC does not indicate APE in Sec. IV. The discussion of our results is presented in Sec. V. The conclusion is given in Sec. VI.

II. MODEL

We describe a DN/SC junction on a two-dimensional tight-binding lattice as shown in Fig. 1, where L is the length of a DN, W is the width of a junction, x (y) is the unit vector in the x (y) direction, and a vector $\mathbf{r} = j\mathbf{x} + m\mathbf{y}$ indicates a lattice site. The Hamiltonian consists of four terms,

$$H = H_{\text{kin}} + H_{\text{imp}} + H_{\text{SOI}} + H_{\Delta}. \quad (1)$$

The kinetic energy of an electron is represented by

$$H_{\text{kin}} = -t \sum_{\mathbf{r}, \mathbf{r}'} \sum_{\alpha=\uparrow, \downarrow} (c_{\mathbf{r}, \alpha}^{\dagger} c_{\mathbf{r}', \alpha} + c_{\mathbf{r}', \alpha}^{\dagger} c_{\mathbf{r}, \alpha}) + (4t - \mu) \sum_{\mathbf{r}, \alpha} c_{\mathbf{r}, \alpha}^{\dagger} c_{\mathbf{r}, \alpha}, \quad (2)$$

where t is the nearest-neighbor hopping integral, μ is the chemical potential, and $c_{\mathbf{r}, \alpha}^{\dagger}$ ($c_{\mathbf{r}, \alpha}$) is the creation (annihilation) operator of an electron with spin α at \mathbf{r} . The second term represents the random impurity potential in a normal metal,

$$H_{\text{imp}} = \sum_{j=1}^L \sum_{m=1}^W \sum_{\alpha} V_{\mathbf{r}} c_{\mathbf{r}, \alpha}^{\dagger} c_{\mathbf{r}, \alpha}, \quad (3)$$

where $V_{\mathbf{r}}$ is potential given randomly in the range of $-V_{\text{imp}}/2 \leq V_{\mathbf{r}} \leq V_{\text{imp}}/2$ by using random numbers with uniform distribution. All the conductances shown below are obtained by averaging the conductance over a number of different samples. The ensemble average of the conductance is insensitive to the types of the random numbers. Thus, we would reach the same conclusions even if we used a random number with Gaussian distribution. The superconducting segment $j \geq L + 1$ is free from potential disorder. We consider the SOI in a SC as

$$H_{\text{SOI}} = \frac{i}{2} \sum_{\mathbf{r}, \alpha, \alpha'} [\lambda_x (c_{\mathbf{r}, \alpha}^{\dagger} c_{\mathbf{r}+x, \alpha'} - c_{\mathbf{r}+x, \alpha}^{\dagger} c_{\mathbf{r}, \alpha'}) (\sigma_y)_{\alpha, \alpha'} - \lambda_y (c_{\mathbf{r}, \alpha}^{\dagger} c_{\mathbf{r}+y, \alpha'} - c_{\mathbf{r}+y, \alpha}^{\dagger} c_{\mathbf{r}, \alpha'}) (\sigma_x)_{\alpha, \alpha'}], \quad (4)$$

where $\lambda_{x(y)}$ represents the strength of SOI coupled to a momentum k_x (k_y), and σ_i for $i = x, y$, and z represents the Pauli matrix in spin space. In this paper, we mainly consider the three types SOI

$$(\lambda_x, \lambda_y) = (\lambda, 0), \quad x \text{ type}, \quad (5a)$$

$$(\lambda_x, \lambda_y) = (0, \lambda), \quad y \text{ type}, \quad (5b)$$

$$(\lambda_x, \lambda_y) = (\lambda, \lambda), \quad \text{Rashba}. \quad (5c)$$

Here x -type and y -type SOIs are a source of the persistent spin helix [37–39]. The last one is the Rashba spin-orbit interaction. The pair potential for a spin-singlet $d_{x^2-y^2}$ symmetry class is described by

$$H_{\Delta} = \frac{\Delta}{2} \sum_{j=L+1}^{\infty} \sum_{m=1}^W (c_{\mathbf{r}+x, \uparrow}^{\dagger} c_{\mathbf{r}, \downarrow}^{\dagger} + c_{\mathbf{r}, \uparrow}^{\dagger} c_{\mathbf{r}+x, \downarrow}^{\dagger} - c_{\mathbf{r}+y, \uparrow}^{\dagger} c_{\mathbf{r}, \downarrow}^{\dagger} - c_{\mathbf{r}, \uparrow}^{\dagger} c_{\mathbf{r}+y, \downarrow}^{\dagger} + \text{H.c.}), \quad (6)$$

where Δ is the amplitude of the pair potential. For a spin-singlet s -wave SC, we choose

$$H_{\Delta} = \Delta \sum_{j=L+1}^{\infty} \sum_{m=1}^W [c_{\mathbf{r}, \uparrow}^{\dagger} c_{\mathbf{r}, \downarrow}^{\dagger} + \text{H.c.}]. \quad (7)$$

The differential conductance of a DN/SC junction is calculated based on the Blonder-Tinkham-Klapwijk formula [40],

$$G_{\text{NS}}(eV) = \frac{e^2}{h} \sum_{l, l', \alpha, \alpha'} [\delta_{l, l'} \delta_{\alpha, \alpha'} - |r_{l, \alpha; l', \alpha'}^{\text{ec}}|^2 + |r_{l, \alpha; l', \alpha'}^{\text{he}}|^2]_{E=eV}, \quad (8)$$

where $r_{l, \alpha; l', \alpha'}^{\text{ec}}$ is the normal reflection coefficient from the l' th propagating channel with spin α' in the electron branch to the l th propagating channel with spin α in the electron branch, whereas $r_{l, \alpha; l', \alpha'}^{\text{he}}$ is the Andreev reflection coefficient from the l' th propagating channel with spin α' in the electron branch to the l th propagating channel with spin α in the hole branch. These reflection coefficients are calculated by using the recursive Green's function method [41,42]. The normal state conductance of a DN is calculated based on the Landauer formula

$$G_{\text{N}} = \frac{e^2}{h} \sum_{l, l', \alpha, \alpha'} |t_{l, \alpha; l', \alpha'}|^2, \quad (9)$$

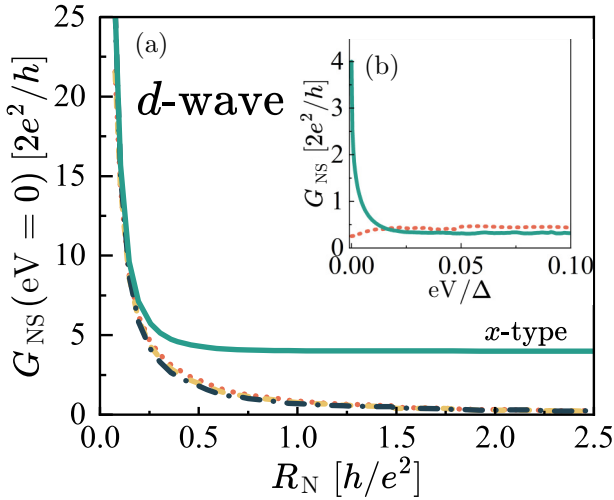


FIG. 2. (a) The results for a $d_{x^2-y^2}$ -wave junction. The zero-bias differential conductance is plotted as a function of the normal state resistance R_N in a normal metal. The results for x -type SOI decrease to $4G_0$ at $R_N \rightarrow \infty$. The results for y -type SOI, those for Rashba SOI, and those without SOI almost overlap with one another. They decrease to zero at $R_N \rightarrow \infty$. (b) The differential conductance is plotted as a function of the bias voltage at $R_N = 4.5(h/e^2)$.

where $t_{l,\alpha;l',\alpha'}$ is the normal transmission coefficient from the l' th propagating channel with spin α' to the l th propagating channel with spin α through a DN.

In this paper, the energy is measured in units of t . We fix several parameters: $\mu = 2t$, $\Delta = 0.1t$, $L = 50$, and $W = 25$. The pair potential is not determined self-consistently because the gap equation always has a stable solution even in the presence of SOIs. We use typically 100–500 different samples for the ensemble averaging over random impurity configurations.

III. RESULTS

A. d wave

We first study the conductance in a junction consisting of a $d_{x^2-y^2}$ wave SC. In Fig. 2(a), the zero-bias conductance $G_{NS}(0)$ is plotted as a function of the normal state resistance of a DN, $R_N = G_N^{-1}$, for $\lambda = 0.5t$, where the vertical axis is normalized to $G_0 = 2e^2/h$. The conductance is averaged over 100 samples with different random configurations. The results are separated into two groups: x -type SOI and other cases. The results for the y -type SOI, those for Rashba SOI, and those without SOI almost overlap with one another. They decrease with increasing R_N and vanish for large R_N . The effects of the SOI on the zero-bias conductance are negligible for y -type SOI and Rashba SOI. These behaviors can be explained by the classical expression of the total resistance of the resistors in series. Because the resistance in a SC is zero, the total resistance of the junction would be given by

$$R_{NS} = R_B + \tilde{R}_N = G_{NS}^{-1}, \quad (10)$$

where R_B is the normal resistance due to the potential barrier at the DN/SC interface. In the present results the Sharvin resistance replaces R_B because we do not introduce the potential barrier at the interface. The usual proximity effect decreases

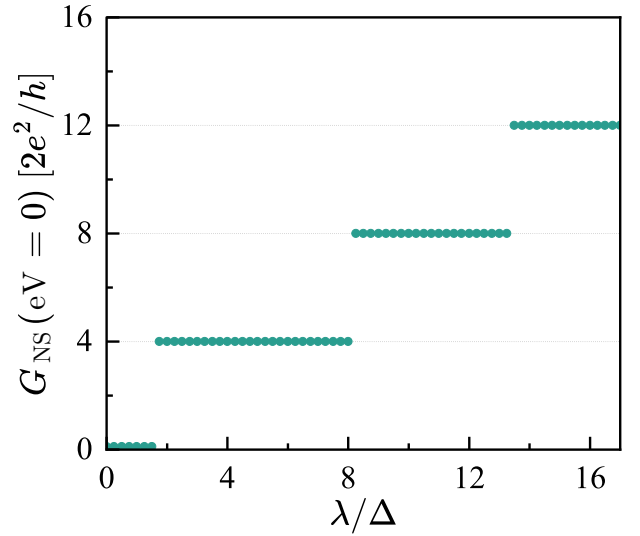


FIG. 3. The zero-bias conductance of a $d_{x^2-y^2}$ -wave junction for x -type SOI is plotted as a function of the strength of SOI λ at $R_N = 4.5G_0^{-1}$.

the resistance in a DN only slightly to $\tilde{R}_N \lesssim R_N$. As a result, the relation $G_{NS} \rightarrow 0$ is expected in the limit of $R_N \rightarrow \infty$. On the other hand, the conductance for x -type SOI deviates from such a relationship and saturates at a finite value of $4G_0$ for large R_N . Such unusual behavior is an aspect of the APE [26]. The resonant states at zero energy form the perfect transmission channels in a DN. In Fig. 2(a), the number of such zero-energy states is 4. In Fig. 2(b), the differential conductance G_{NS} at $R_N = 4.5(h/e^2)$ is plotted as a function of the bias voltage eV . The conductance for the x -type SOI decreases rapidly with increasing eV because the perfect resonant transmission occurs only at zero bias. As a consequence, the results for the x -type SOI exhibit a sharp peak at zero bias. For comparison, we plot the results for Rashba SOI in Fig. 2(b) with a broken line. The conductance exhibits no distinct peak structures around zero bias.

The zero-bias conductance in the limit of $R_N \rightarrow \infty$ depends on the amplitude of the x -type SOI λ as shown in Fig. 3, where $G_{NS}(0)$ is plotted as a function of λ . The conductance remains zero for $\lambda < 0.175t$ and jumps to a finite value of $4G_0$ at $\lambda = 0.175t$. Such steplike behavior is observed also at $\lambda = 0.85t$ and $\lambda = 1.35t$. The conductance is quantized at the steps $4G_0$, $8G_0$, and $12G_0$. As we will discuss in Sec. IV, the minimum value of the conductance is given by $G_0 \mathcal{N}_{ZES}$, where \mathcal{N}_{ZES} is the number of zero-energy states that form the perfect transmission channels in a DN. The results indicate that \mathcal{N}_{ZES} changes discontinuously at factors of 4.

B. s wave

Second, we discuss the absence of the APE in a DN/SC junction for an s -wave symmetry. In Fig. 4(a), we plot the zero-bias conductance as a function of R_N for an s -wave superconductor including x -type SOI, y -type SOI, and Rashba SOI with $\lambda = 0.5t$. We also plot the results without SOI $\lambda = 0$ in the figure. All of the results overlap with one another, which indicates that the effects of SOI on the conductance

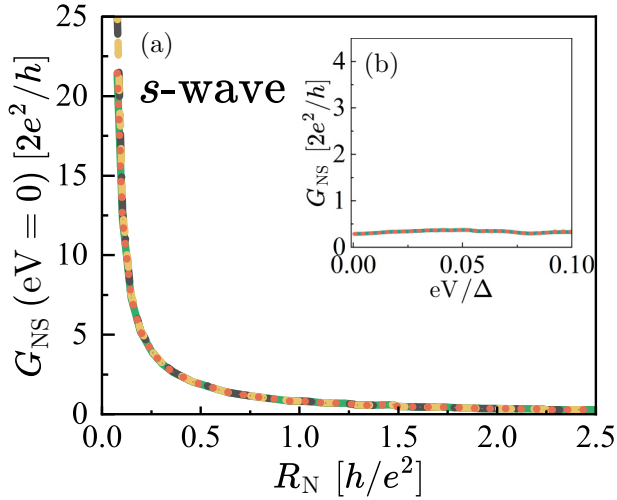


FIG. 4. (a) The results for an s -wave DN/SC junction. The zero-bias differential conductance is plotted as a function of normal state resistance R_N in a normal metal. Although we consider x and y type SOIs, Rashba SOI, and absence of SOI, all the results almost overlap with one another. (b) The differential conductance is plotted as a function of the bias voltage at $R_N = 4.5(h/e^2)$.

are negligible in an s -wave junction. In all cases, the zero-bias conductance decreases to zero with increasing R_N . In the inset, Fig. 4(b), we also plot the differential conductance G_{NS} at $R_N = 4.5 G_0^{-1}$ as a function of the bias voltage. The results show that the conductance is insensitive to the bias voltage. The results in Fig. 4 suggest that s -wave superconductor junctions do not indicate the APE regardless of the type of SOI. We will discuss the reasons in Sec. IV.

IV. MODIFIED PAIR POTENTIAL AND INDEX

There are two conditions for a superconductor that indicates the APE: the presence of the usual proximity effect in a DN and the existence of the Andreev bound states at its surfaces parallel to the y direction [3]. We first consider a spin-singlet even-parity SC without SOIs. The BdG Hamiltonian is such a SC can be block diagonalized into two 2×2 Hamiltonian. When the pair potential in one spin sector is $\Delta(\mathbf{k})$, that in the other is $-\Delta(\mathbf{k})$. A SC causes the usual proximity effect when its pair potential satisfies [5]

$$\Delta(k_x, -k_y) \neq -\Delta(k_x, k_y), \quad (11)$$

where k_x and k_y are the wave numbers on the Fermi surface. The pair potentials considered in this paper are described by

$$\Delta(\mathbf{k}) = \begin{cases} \Delta(k_x^2 - k_y^2)/k_F^2, & d_{x^2-y^2} \text{ wave,} \\ \Delta, & s \text{ wave,} \end{cases} \quad (12)$$

where k_F is the Fermi wave number on the isotropic Fermi surface. Both the $d_{x^2-y^2}$ -wave pair potential and the s -wave pair potential satisfy Eq. (11). In the junction geometry in Fig. 1, the wave number in the y direction, k_y , indicates a transport channel. Meanwhile, the presence of the surface Andreev bound states is ensured when the pair potential satisfies [8,9]

$$\Delta(k_x, k_y)\Delta(-k_x, k_y) < 0. \quad (13)$$

Either the $d_{x^2-y^2}$ -wave pair potential or the s -wave pair potential does not satisfy the condition in the absence of SOIs [3]. Thus spin-singlet SCs do not indicate the APE in the absence of SOIs.

Second, we discuss how SOI modifies the pair potential on the Fermi surface of a $d_{x^2-y^2}$ -wave SC. The Hamiltonian considered in this paper is represented in continuous space,

$$H_{\text{BdG}}(\mathbf{k}) = (\xi_{\mathbf{k}} - \lambda_x k_x \hat{\sigma}_y) \hat{\tau}_z + \lambda_y k_y \hat{\sigma}_x - \Delta(\mathbf{k}) \hat{\sigma}_y \hat{\tau}_y, \quad (14)$$

which enables us to derive the analytical expression of the quantized value of the conductance minimum. We first apply a unitary transformation to H_{BdG} to diagonalize the normal state Hamiltonian. For x -type SOI with Eq. (5a), we find

$$H_{\text{BdG}}(\mathbf{k}) = \check{U} \begin{bmatrix} \xi_{\mathbf{k}} + \lambda k_x & 0 & 0 & \Delta(\mathbf{k}) \\ 0 & \xi_{\mathbf{k}} - \lambda k_x & -\Delta(\mathbf{k}) & 0 \\ 0 & -\Delta(\mathbf{k}) & -\xi_{\mathbf{k}} + \lambda k_x & 0 \\ \Delta(\mathbf{k}) & 0 & 0 & -\xi_{\mathbf{k}} - \lambda k_x \end{bmatrix} \times \check{U}^\dagger, \quad (15)$$

$$\check{U} = \frac{1}{\sqrt{2}}(1 + i\hat{\sigma}_x \hat{\tau}_z). \quad (16)$$

The Hamiltonian is separated into the two 2×2 Hamiltonian in this representation. The x -type SOI divides the Fermi surface into two: one moves toward the $+k_x$ direction and the other moves toward the $-k_x$ direction. The Fermi surface derived from the dispersion $\xi_{\mathbf{k}} + \lambda k_x$ ($\xi_{\mathbf{k}} - \lambda k_x$) is illustrated as an open circle labeled by the left (right) Fermi surface in Figs. 5(a) and 5(d), where a black dot indicates the Γ point in the Brillouin zone (i.e., $\mathbf{k} = 0$). The pair potentials for $d_{x^2-y^2}$ -wave symmetry are shown on the two Fermi surfaces in Fig. 5(a). In Fig. 5(a), Eq. (13) is satisfied at the shaded domains between the two dotted lines, where k_y in such domains satisfies Eq. (B4). The one-dimensional winding number at fixed k_y is defined by [43]

$$\mathcal{W}(k_y) \equiv -\frac{1}{4\pi i} \int_{-\infty}^{\infty} dk_x I(k_y), \quad (17)$$

$$I(k_y) = \text{Tr}[\hat{\tau}_x H_{\text{BdG}}^{-1} \partial_{k_x} H_{\text{BdG}}], \quad (18)$$

$$\{H_{\text{BdG}}, \hat{\tau}_x\}_+ = 0. \quad (19)$$

The one-dimensional winding number is calculated as

$$\mathcal{W}(k_y) = \mathcal{W}(-k_y) = 2, \quad (20)$$

for all k_y in the shaded domains in Fig. 5(a). As a result,

$$\mathcal{N}_{\text{ZES}} = \sum_{k_y} \mathcal{W}(k_y) \quad (21)$$

remains a finite value. This index represents the number of zero-energy states which form the resonant transmission channels in a DN [26]. The conductance for large enough R_N is quantized at

$$G_{\text{NS}} = G_0 \times |\mathcal{N}_{\text{ZES}}|. \quad (22)$$

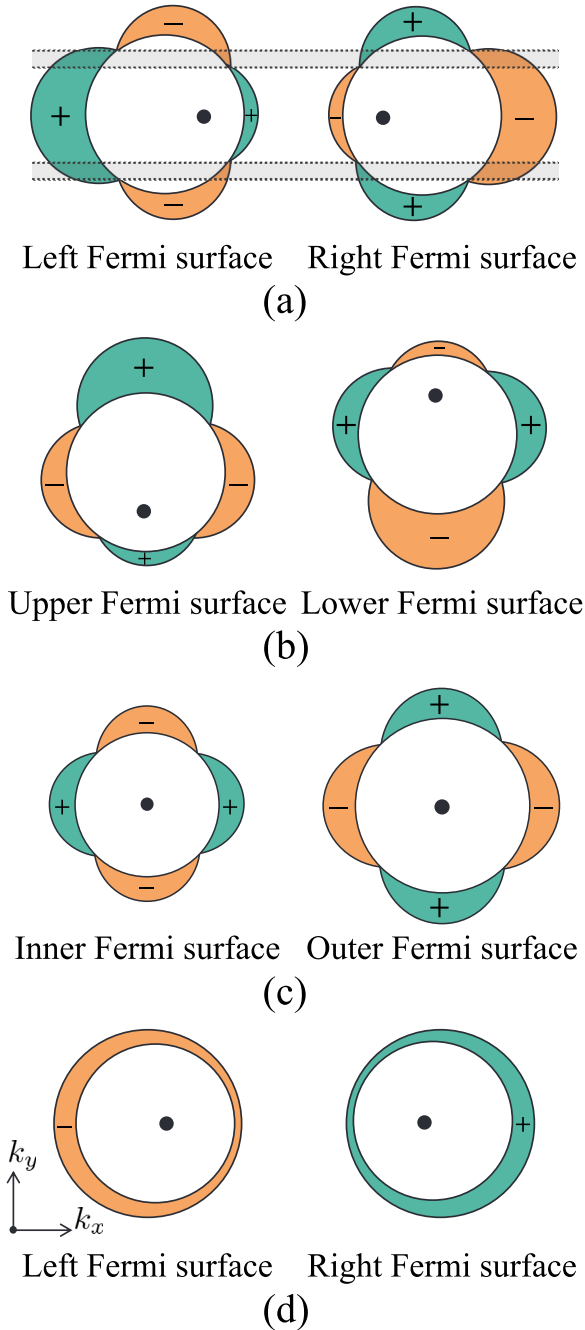


FIG. 5. The pair potentials of a $d_{x^2-y^2}$ -wave SC on the Fermi surface with (a) x -type SOI, (b) y -type SOI, and (c) Rashba SOI. The black dot in the figure indicates the Γ point ($k=0$). In the domains between the two dotted lines in (a), the condition $\Delta(k_x, k_y)\Delta(-k_x, k_y) < 0$ is satisfied. In (d), the pair potentials of an s -wave SC are illustrated for x -type SOI.

Thus $|\mathcal{N}_{ZES}|$ increases by 4 with increasing λ as shown in Fig. 3. The index is approximately calculated as

$$\mathcal{N}_{ZES} \approx \left[2N_c \frac{\lambda k_F}{\mu} \right]_G, \quad (23)$$

where $[\dots]_G$ means the integer part of the argument, and N_c is the number of propagating channels on the Fermi surface per spin. The expression is valid for $\lambda k_F \ll \mu$. In Appendix B, we

supply details of the derivation of Eq. (23) and explain why we choose $\hat{\tau}_x$ as a chiral operator in Eq. (19). Thus the quantized value of the conductance increases monotonically with increasing λ . In Fig. 3, the conductance jumps discontinuously because the number of propagating channels are limited for $W = 25$ in the numerical simulation. Thus, G_{NS} will become a smoother function of λ for a wider junction with $N_c \gg 1$. In Fig. 5(d), we also illustrate the pair potential for an s -wave SC with the x -type SOI. Although the SOI splits the Fermi surface into two and modifies the amplitudes of the pair potentials, it does not change the sign of the pair potentials. Therefore, the APE is absent in s -wave junctions. The SOIs generate spin-triplet odd-parity Cooper pairs as a subdominant pairing correlation from the spin-singlet pair potentials. This happens in both a d -wave SC and an s -wave SC. The induced spin-triplet Cooper pairs are expected to modify the properties of a spin-singlet SC to those in spin-triplet SC. The APE is a spin-triplet specific phenomenon. However, the appearance of the spin-triplet pairing correlation is only a necessary condition for the APE. Our results show that the APE requires the sign change in the pair potential.

Third, we discuss the effects of y -type SOI with Eq. (5b) and those of Rashba SOI with Eq. (5c) on the pair potentials for $d_{x^2-y^2}$ -wave symmetry. The y -type SOI shifts the Fermi surface in the $+k_y$ ($-k_y$) direction and forms the upper (lower) Fermi surface as shown in Fig. 5(b). The condition (13) is not satisfied because the pair potentials are always even functions of k_x . In the presence of Rashba SOI, the Fermi surface derived from the dispersion $\xi_k + \lambda|\mathbf{k}|$ ($\xi_k - \lambda|\mathbf{k}|$) forms the outer (inner) Fermi surface as illustrated in Fig. 5(c). The condition Eq. (13) is not satisfied for the Rashba SOI because the pair potentials are always even functions of k_x . Therefore, the APE is absent in these cases.

At the end of this section, we briefly discuss the effects of the misorientation of the $d_{x^2-y^2}$ -wave pair potential on the APE. The pair potential in Eq. (12) is expressed as $\Delta \cos 2\theta$ with $k_x = k_F \cos \theta$ and $k_y = k_F \sin \theta$. When the pair potential is oriented as $\Delta \cos 2(\theta - \beta)$ with $0 \leq \beta < \pi/4$, the index in Eq. (23) is calculated as

$$\mathcal{N}_{ZES} \approx \left[2N_c \frac{\lambda k_F}{\mu} \cos 2\beta \right]_G. \quad (24)$$

Therefore, the APE is robust to small misorientations of the pair potential.

V. DISCUSSION

Finally, we discuss a relation between the conclusions of this paper and the experimental results in a T-shaped $\text{CoSi}_2/\text{TiO}_2$ junction on a Si substrate [32]. In the experiment, a clear zero-bias peak is observed in the conductance spectra, which means that a spin-triplet odd-parity (such as p -wave and f -wave) Cooper pair is definitely present in the thin film of CoSi_2 . The spin-triplet odd-parity pairing correlation makes the SC topologically nontrivial, which accommodates zero-energy quasiparticles at its surface. Majorana zero modes are a special case of such zero-energy states. The penetration of the zero-energy states into a dirty normal metal causes the APE. The zero-bias conductance peak in a T-shaped junction reflects the enhancement of the density of states at zero energy

due to the penetration [10]. The index \mathcal{N}_{ZES} represents the degree of the degeneracy of such zero energy states in a dirty normal metal. We note, however, that spin-singlet s -wave superconductivity has been well established in bulk CoSi_2 . Therefore, theories are necessary that explain why spin-triplet Cooper pairs are present in CoSi_2 . The experiment also reported strong SOIs at the interface between CoSi_2 and the Si substrate [33,34].

To explain the experimental results, we are compelled to consider symmetries other than s -wave symmetries for the pair potentials in CoSi_2 thin films on Si substrates, as listed below.

(i) The pair potential belongs to the spin-triplet odd-parity class.

(ii) Two pair potentials coexist. One belongs to the spin-triplet odd-parity class. The other belongs to the spin-singlet even-parity class.

(iii) Although the pair potential belongs to the spin-singlet class, SOIs generate spin-triplet Cooper pairs.

If (i) is correct, our previous theory [10] explains well the zero-bias peak in the experiment. The authors of Refs. [44,45] consider (ii) and assume the effective attractive interactions at a p -wave channel under the strong SOIs. The zero-bias peak in a T-shaped junction is explained only when the amplitude of the spin-triplet pair potential is larger than that of the spin-singlet pair potential. However, both (i) and (ii) require the spin-triplet p -wave pair potential. At present, we do not know of any p -wave attractive interactions between two electrons in CoSi_2 . In this paper, we considered a different scenario of (iii) where the SC has only a spin-singlet pair potential. We have shown in this paper that an s -wave SC does not indicate the APE with any types of SOIs. The spin-singlet d -wave pair potential with a specific SOI is necessary to explain the experiment. The realization of a spin-singlet d -wave order parameter might be easier than that of spin-triplet p -wave one. However, we are not sure what mediates d -wave attractive interactions and if x -type SOI is realized in CoSi_2 . Therefore, the puzzle has not been solved yet.

VI. CONCLUSION

We theoretically studied the effects of the spin-orbit interaction (SOI) in a spin-singlet superconductor on the low-energy transport properties in a dirty normal-metal/superconductor junction as shown in Fig. 1. The differential conductance is calculated based on the Blonder-Tinkham-Klapwijk formula and the transport coefficients are calculated numerically by using the recursive Green's function method. We consider two types of pair potentials, s - and d -wave symmetry, and three types of SOI, x type, y type, and Rashba type. Our results demonstrate that a d -wave SC with x -type SOI exhibits the anomalous proximity effect (APE), whereas a d -wave SC with y -type SOI and that with Rashba SOI do not indicate the APE. The numerical results also show that an s -wave SC with any type of SOI does not show the APE. We explain the numerical results by analyzing how SOIs change the sign of the pair potentials on the Fermi surface. Our findings provide an experimental setup for realizing an artificial spin-triplet SC.

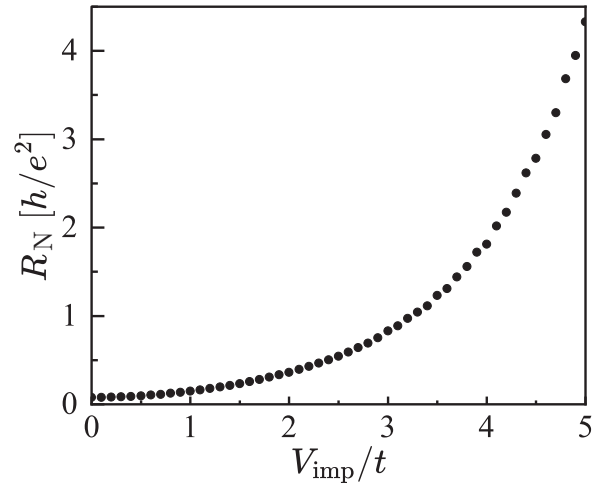


FIG. 6. The conductance is plotted as a function of the normal state resistance in a normal metal, R_N , in Figs. 2 and 4.

ACKNOWLEDGMENTS

The authors are grateful to Y. Tanaka, S. Kirchner, and S. Kobayashi for useful discussions. J.L. is supported by the Asahi Glass Foundation (Grant No. S20K01). S. I. is supported by a Grant-in-Aid for Early-Career Scientists (JSPS KAKENHI Grant No. JP24K17010).

DATA AVAILABILITY

The data that support the findings of this article are openly available [46].

APPENDIX A: RESISTANCE IN NORMAL STATE

The conductance is plotted as a function of the normal state resistance in a normal metal, R_N , in Figs. 2 and 4. Here, we explain how to obtain R_N in the numerical simulation. We calculate the normal conductance G_N in Eq. (9) for a disordered normal metal for $\mu = 2t$, $L = 50$, and $W = 25$. After repeating the calculation at a fixed V_{imp} over a number of different samples with different random potential configurations, R_N is defined by the inverse of the ensemble average of G_N . In Fig. 6, we plot R_N as a function of V_{imp} .

R_N increases with increasing V_{imp} . In Figs. 2 and 4, we calculate the ensemble average of G_{NS} as a function of V_{imp} and plot the results as a function of R_N .

APPENDIX B: ATIYAH-SINGER INDEX

We briefly summarize the relation between the quantized value of the zero-bias conductance and an index \mathcal{N}_{ZES} . Let us begin with a BdG Hamiltonian for a spin-singlet SC with the x -type SOI in Eq. (14). The wave number on the Fermi surface is determined by

$$\xi_k + s \lambda k_x = 0, \quad s = \pm 1, \quad (\text{B1})$$

where $s = 1$ (-1) corresponds to the Fermi surface shifted to the left (right) in Fig. 5(a). The wave numbers in the two

directions satisfy

$$(k_x + s\tilde{\lambda}k_F)^2 + k_y^2 = (1 + \tilde{\lambda}^2)k_F^2, \quad (\text{B2})$$

$$\tilde{\lambda} \equiv \frac{\lambda k_F}{2\mu} \ll 1. \quad (\text{B3})$$

The x -type SOI shifts the center of the Fermi surface to $\pm\tilde{\lambda}k_F$ on the k_x axis. The pair potential of a $d_{x^2-y^2}$ -wave SC on the Fermi surface has nodes at $k_x = \pm k_y$. As a result, Eq. (13) is satisfied at the channels

$$\frac{k_F}{2}(\sqrt{\tilde{\lambda}^2 + 2} - \tilde{\lambda}) \leq |k_y| \leq \frac{k_F}{2}(\sqrt{\tilde{\lambda}^2 + 2} + \tilde{\lambda}), \quad (\text{B4})$$

for both the left and right Fermi surfaces. A schematic figure of the pair potentials is shown in Fig. 5(a). The pair potential indicated by shaded area in Fig. 5(a) satisfies Eq. (13), indicating the appearance of surface Andreev bound state at each propagating channel. The number of such ZESs for the two spin sectors is estimated as

$$N = [4N_c\tilde{\lambda}]_G, \quad (\text{B5})$$

where $N_c = Wk_F/\pi$ is the number of propagating channels for each spin sector, W is the width of the SC in the y direction, and $[\dots]_G$ means the Gauss symbol providing the integer part of a number. As a result, the number of Andreev bound states at zero-energy is N at a clean surface of a $d_{x^2-y^2}$ -wave SC with the x -type SOI. In other words, N represents the degree of the degeneracy of zero-energy states at a surface of a SC. Such a high degeneracy is a result of translational symmetry in the y direction of a clean SC. In a clean normal-metal/SC junction, the zero-energy states penetrate into the clean normal metal and form the perfect transmission channels.

To discuss effects of random potentials in a normal metal attached to a SC, the analysis of chiral property of zero-energy states is necessary [25,26]. The BdG Hamiltonian in Eq. (14) preserves chiral symmetry in Eq. (19). Since $\hat{\tau}_x^2 = 1$, the eigenvalues of $\hat{\tau}_x$ are either 1 (positive chirality) or -1 (negative chirality). It is known that a zero-energy state of H_{BdG} is the eigenstate of $\hat{\tau}_x$. Therefore, such a zero-energy state has either positive chirality or negative chirality. The wave functions of the zero-energy states are calculated as

$$\psi_1 = \begin{pmatrix} i \\ 1 \\ -i \\ -1 \end{pmatrix} A e^{ik_y y} f(x), \quad \psi_2 = \begin{pmatrix} 1 \\ i \\ -1 \\ -i \end{pmatrix} A e^{ik_y y} f(x), \quad (\text{B6})$$

where A is a normalization constant and $f(x)$ is a function localizing at a surface of a SC. It is easy to confirm that all of the zero-energy states belong to the negative chirality, as it satisfies $\hat{\tau}_x \psi_j = -\psi_j$ for $j = 1$ and 2 . The Atiyah-Singer index is defined by

$$\mathcal{N}_{\text{ZES}} = N_+ - N_-, \quad (\text{B7})$$

where N_+ (N_-) is the number of zero-energy states belonging to positive (negative) chirality. Therefore, the index is calculated as

$$|\mathcal{N}_{\text{ZES}}| = [4N_c\tilde{\lambda}]_G. \quad (\text{B8})$$

The index \mathcal{N}_{ZES} is an invariant in the presence of chiral symmetry of the Hamiltonian. Here we calculate the index in a

clean SC by assuming translational symmetry in the y direction. The index remains unchanged even when the random impurity potential

$$H_{\text{imp}} = V(\mathbf{r}) \tau_z \quad (\text{B9})$$

enters the Hamiltonian in Eq. (14). This is because the random potential preserves chiral symmetry. In physics, $|\mathcal{N}_{\text{ZES}}|$ represents the number of zero-energy states that penetrate into a dirty normal metal while retaining their high degeneracy and form the perfect transmission channels. The electric current through such perfect transmission channels is independent of R_N , whereas the electric current through usual transmission channels decreases with increasing R_N . As a result, the minimum value of the conductance at zero bias is described by Eq. (22) [25,26].

Finally, we explain why we choose $\hat{\tau}_x$ as a chiral operator in Eq. (19). A spin-singlet superconductor with spin-orbit interactions preserves time-reversal symmetry,

$$\mathcal{T} H_{\text{BdG}}(\mathbf{k}) \mathcal{T}^{-1} = H_{\text{BdG}}(\mathbf{k}), \quad \mathcal{T} = i\hat{\sigma}_y \mathcal{K}, \quad (\text{B10})$$

where \mathcal{K} means taking complex conjugation and $\mathbf{k} \rightarrow -\mathbf{k}$. The Hamiltonian preserves particle-hole symmetry simultaneously,

$$\mathcal{P} H_{\text{BdG}}(\mathbf{k}) \mathcal{P}^{-1} = -H_{\text{BdG}}(\mathbf{k}), \quad \mathcal{P} = \hat{\tau}_x \mathcal{K}. \quad (\text{B11})$$

As a result of combining these symmetries, the BdG Hamiltonian anticommutes to $\tau_x \sigma_y$:

$$\Gamma H_{\text{BdG}}(\mathbf{k}) \Gamma = -H_{\text{BdG}}(\mathbf{k}), \quad \Gamma = \hat{\tau}_x \hat{\sigma}_y. \quad (\text{B12})$$

It is possible to calculate the one-dimensional winding number $\mathcal{W}'(k_y)$ for each k_y according to the definition in Eqs. (17)–(19), replacing $\hat{\tau}_x$ by $\hat{\tau}_x \hat{\sigma}_y$. However, two of authors have shown that the index \mathcal{N}_{ZES} in Eq. (21) calculated from such winding numbers is always zero [27] because of the relation $\mathcal{W}'(k_y) = -\mathcal{W}'(-k_y)$. This conclusion is derived only from the symmetry relationships of the BdG Hamiltonian belonging to class DIII. The anomalous proximity effect is a characteristic phenomenon of a superconductor whose Hamiltonian belongs to class BDI. At $\lambda_y = 0$, the BdG Hamiltonian preserves spin-rotation symmetry around the y axis

$$\hat{\sigma}_y H_{\text{BdG}}(\mathbf{k}) \hat{\sigma}_y = H_{\text{BdG}}(\mathbf{k}). \quad (\text{B13})$$

By combining such spin-rotation symmetry and time-reversal symmetry, we define a time-reversal like operator and a chiral operator as

$$\mathcal{T}_+ = \hat{\sigma}_y \hat{\sigma}_y \mathcal{K} = \mathcal{K}, \quad \mathcal{T}_+^2 = 1, \quad (\text{B14})$$

$$\Gamma_{\text{BDI}} = \mathcal{T}_+ \mathcal{P} = \hat{\tau}_x. \quad (\text{B15})$$

We find that the BdG Hamiltonian at $\lambda_y = 0$ anticommutes to $\hat{\tau}_x$. At $\lambda_x = 0$, combining spin-rotation symmetry around the x axis,

$$\hat{\tau}_z \hat{\sigma}_x H_{\text{BdG}}(\mathbf{k}) \hat{\sigma}_x \hat{\tau}_z = H_{\text{BdG}}(\mathbf{k}), \quad (\text{B16})$$

and time-reversal symmetry, we define another time-reversal-like operator and a chiral operator:

$$\mathcal{T}_+ = \hat{\sigma}_x \hat{\tau}_z \hat{\sigma}_y \mathcal{K}, \quad \mathcal{T}_+^2 = 1, \quad (\text{B17})$$

$$\Gamma_{\text{BDI}} = \mathcal{T}_+ \mathcal{P} = \hat{\tau}_y \hat{\sigma}_z. \quad (\text{B18})$$

As a result, we reach the anticommutation relation

$$\hat{\tau}_y \hat{\sigma}_z H_{\text{BdG}}(\mathbf{k}) \hat{\sigma}_z \hat{\tau}_y = -H_{\text{BdG}}(\mathbf{k}). \quad (\text{B19})$$

The winding number by using such a chiral operator is zero for all propagating channels because the pair potential at $\lambda_x = 0$ in Fig. 5(b) is always an even function of k_x .

APPENDIX C: x -TYPE SOI TO RASHBA SOI

We briefly discuss the effects of the y -type SOI introduced in addition to the x -type SOI. The BdG Hamiltonian in continuous space is given in Eq. (14) with $\lambda_z \neq 0$ and $\lambda_y \neq 0$. It is easy to confirm that the BdG Hamiltonian does not preserve chiral symmetry in Eq. (19). Therefore, the index \mathcal{N}_{ZES} can no longer be defined and the conductance deviates from its quantized value. In Fig. 7, the conductance is plotted as a function of the bias voltage for several choices of R_N . We choose $(\lambda_x, \lambda_y) = (0.5t, 0)$ in (a) and $(\lambda_x, \lambda_y) = (0.5t, 0.05t)$ in (b). The minimum value of the zero-bias conductance is quantized as Eq. (22) in Fig. 7(a) irrespective of R_N . When

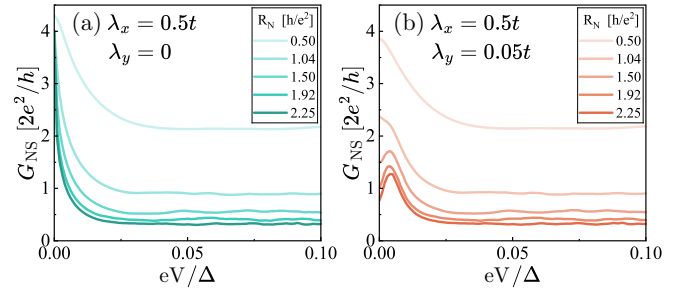


FIG. 7. The conductance of a $d_{x^2-y^2}$ -wave junction is plotted as a function of the bias voltage for several R_N . The results for the x -type SOI at $\lambda_x = 0.5t$ are shown in (a). In (b), we choose $\lambda_x = 0.5t$ and $\lambda_y = 0.05t$.

we add the y -type SOI, the zero-bias conductance decreases gradually with increasing R_N as shown in Fig. 7(b). When λ_y is increased to λ_x , the results for Rashba SOI in Fig. 2 do not exhibit any indication of the APE. Thus, the APE is fragile under perturbations that break chiral symmetry.

- [1] Y. Tanaka and S. Kashiwaya, Anomalous charge transport in triplet superconductor junctions, *Phys. Rev. B* **70**, 012507 (2004).
- [2] Y. Tanaka, S. Kashiwaya, and T. Yokoyama, Theory of enhanced proximity effect by midgap Andreev resonant state in diffusive normal-metal/triplet superconductor junctions, *Phys. Rev. B* **71**, 094513 (2005).
- [3] Y. Asano, Y. Tanaka, and S. Kashiwaya, Anomalous Josephson effect in p -wave dirty junctions, *Phys. Rev. Lett.* **96**, 097007 (2006).
- [4] Y. Asano, Y. Tanaka, T. Yokoyama, and S. Kashiwaya, Josephson current through superconductor/diffusive-normal-metal/superconductor junctions: Interference effects governed by pairing symmetry, *Phys. Rev. B* **74**, 064507 (2006).
- [5] Y. Asano, Disappearance of ensemble-averaged Josephson current in dirty superconductor-normal-superconductor junctions of d -wave superconductors, *Phys. Rev. B* **64**, 014511 (2001).
- [6] L. J. Buchholtz and G. Zwicknagl, Identification of p -wave superconductors, *Phys. Rev. B* **23**, 5788 (1981).
- [7] C.-R. Hu, Midgap surface states as a novel signature for $d_{xy}^2-x_b^2$ -wave superconductivity, *Phys. Rev. Lett.* **72**, 1526 (1994).
- [8] Y. Tanaka and S. Kashiwaya, Theory of tunneling spectroscopy of d -wave superconductors, *Phys. Rev. Lett.* **74**, 3451 (1995).
- [9] Y. Asano, Y. Tanaka, and S. Kashiwaya, Phenomenological theory of zero-energy Andreev resonant states, *Phys. Rev. B* **69**, 134501 (2004).
- [10] Y. Asano, Y. Tanaka, A. A. Golubov, and S. Kashiwaya, Conductance spectroscopy of spin-triplet superconductors, *Phys. Rev. Lett.* **99**, 067005 (2007).
- [11] Y. Asano, A. A. Golubov, Y. V. Fominov, and Y. Tanaka, Unconventional surface impedance of a normal-metal film covering a spin-triplet superconductor due to odd-frequency Cooper pairs, *Phys. Rev. Lett.* **107**, 087001 (2011).
- [12] G. R. Stewart, Z. Fisk, J. O. Willis, and J. L. Smith, *Possibility of Coexistence of Bulk Superconductivity and Spin Fluctuations in UPt3* (Springer, Dordrecht, 1993), pp. 85–88.
- [13] H. R. Ott, H. Rudigier, Z. Fisk, and J. L. Smith, UBe_{13} : An unconventional actinide superconductor, *Phys. Rev. Lett.* **50**, 1595 (1983).
- [14] S. S. Saxena, P. Agarwal, K. Ahilan, F. M. Grosche, R. K. W. Haselwimmer, M. J. Steiner, E. Pugh, I. R. Walker, S. R. Julian, P. Monthoux, G. G. Lonzarich, A. Huxley, I. Sheikin, D. Braithwaite, and J. Flouquet, Superconductivity on the border of itinerant-electron ferromagnetism in UGe_2 , *Nature (London)* **406**, 587 (2000).
- [15] S. Ran, C. Eckberg, Q.-P. Ding, Y. Furukawa, T. Metz, S. R. Saha, I.-L. Liu, M. Zic, H. Kim, J. Paglione, and N. P. Butch, Nearly ferromagnetic spin-triplet superconductivity, *Science* **365**, 684 (2019).
- [16] L. Jiao, S. Howard, S. Ran, Z. Wang, J. Olivares Rodriguez, M. Sigrist, Z. Wang, N. P. Butch, and V. Madhavan, Chiral superconductivity in heavy-fermion metal UTe_2 , *Nature (London)* **579**, 523 (2020).
- [17] Y. S. Hor, A. J. Williams, J. G. Checkelsky, P. Roushan, J. Seo, Q. Xu, H. W. Zandbergen, A. Yazdani, N. P. Ong, and R. J. Cava, Superconductivity in $\text{Cu}_x\text{Bi}_2\text{Se}_3$ and its implications for pairing in the undoped topological insulator, *Phys. Rev. Lett.* **104**, 057001 (2010).
- [18] S. Sasaki, M. Kriener, K. Segawa, K. Yada, Y. Tanaka, M. Sato, and Y. Ando, Topological superconductivity in $\text{Cu}_x\text{Bi}_2\text{Se}_3$, *Phys. Rev. Lett.* **107**, 217001 (2011).
- [19] M. Sato, Nodal structure of superconductors with time-reversal invariance and Z_2 topological number, *Phys. Rev. B* **73**, 214502 (2006).
- [20] M. Sato and S. Fujimoto, Topological phases of non-centrosymmetric superconductors: Edge states, Majorana fermions, and non-Abelian statistics, *Phys. Rev. B* **79**, 094504 (2009).
- [21] R. M. Lutchyn, J. D. Sau, and S. Das Sarma, Majorana fermions and a topological phase transition in semiconductor-superconductor heterostructures, *Phys. Rev. Lett.* **105**, 077001 (2010).

- [22] Y. Oreg, G. Refael, and F. von Oppen, Helical liquids and Majorana bound states in quantum wires, *Phys. Rev. Lett.* **105**, 177002 (2010).
- [23] Y. Asano and Y. Tanaka, Majorana fermions and odd-frequency Cooper pairs in a normal-metal nanowire proximity-coupled to a topological superconductor, *Phys. Rev. B* **87**, 104513 (2013).
- [24] S. Das Sarma, M. Freedman, and C. Nayak, Majorana zero modes and topological quantum computation, *npj Quantum Inf.* **1**, 15001 (2015).
- [25] S. Ikegaya, Y. Asano, and Y. Tanaka, Anomalous proximity effect and theoretical design for its realization, *Phys. Rev. B* **91**, 174511 (2015).
- [26] S. Ikegaya, S.-I. Suzuki, Y. Tanaka, and Y. Asano, Quantization of conductance minimum and index theorem, *Phys. Rev. B* **94**, 054512 (2016).
- [27] S. Ikegaya, S. Kobayashi, and Y. Asano, Symmetry conditions of a nodal superconductor for generating robust flat-band Andreev bound states at its dirty surface, *Phys. Rev. B* **97**, 174501 (2018).
- [28] J. Alicea, Majorana fermions in a tunable semiconductor device, *Phys. Rev. B* **81**, 125318 (2010).
- [29] J. You, C. H. Oh, and V. Vedral, Majorana fermions in *s*-wave noncentrosymmetric superconductor with Dresselhaus (110) spin-orbit coupling, *Phys. Rev. B* **87**, 054501 (2013).
- [30] J. Lee, S. Ikegaya, and Y. Asano, Odd-parity pairing correlations in a *d*-wave superconductor, *Phys. Rev. B* **103**, 104509 (2021).
- [31] S. Ikegaya, J. Lee, A. P. Schnyder, and Y. Asano, Strong anomalous proximity effect from spin-singlet superconductors, *Phys. Rev. B* **104**, L020502 (2021).
- [32] S.-P. Chiu, C. C. Tsuei, S.-S. Yeh, F.-C. Zhang, S. Kirchner, and J.-J. Lin, Observation of triplet superconductivity in CoSi₂/TiSi₂ heterostructures, *Sci. Adv.* **7**, eabg6569 (2021).
- [33] S.-P. Chiu, C.-J. Wang, Y.-C. Lin, S.-T. Tu, S. K. Sahu, R.-T. Wang, C.-Y. Wu, S.-S. Yeh, S. Kirchner, and J.-J. Lin, Electronic and superconducting properties of CoSi₂ films on silicon an unconventional superconductor with technological potential, *Chin. J. Phys.* **90**, 348 (2024).
- [34] S.-P. Chiu, V. Mishra, Y. Li, F.-C. Zhang, S. Kirchner, and J.-J. Lin, Tuning interfacial two-component superconductivity in CoSi₂/TiSi₂ heterojunctions *via* TiSi₂ diffusivity, *Nanoscale* **15**, 9179 (2023).
- [35] L. F. Mattheiss and D. R. Hamann, Electronic structure and properties of CoSi₂, *Phys. Rev. B* **37**, 10623 (1988).
- [36] K. Tsutsumi, S. Takayanagi, M. Ishikawa, and T. Hirano, Superconductivity of intermetallic compound CoSi₂, *J. Phys. Soc. Jpn.* **64**, 2237 (1995).
- [37] B. A. Bernevig, J. Orenstein, and S.-C. Zhang, Exact SU(2) symmetry and persistent spin helix in a spin-orbit coupled system, *Phys. Rev. Lett.* **97**, 236601 (2006).
- [38] J. Schliemann, Colloquium: Persistent spin textures in semiconductor nanostructures, *Rev. Mod. Phys.* **89**, 011001 (2017).
- [39] M. Kohda and G. Salis, Physics and application of persistent spin helix state in semiconductor heterostructures, *Semicond. Sci. Technol.* **32**, 073002 (2017).
- [40] G. E. Blonder, M. Tinkham, and T. M. Klapwijk, Transition from metallic to tunneling regimes in superconducting microconstrictions: Excess current, charge imbalance, and supercurrent conversion, *Phys. Rev. B* **25**, 4515 (1982).
- [41] P. A. Lee and D. S. Fisher, Anderson localization in two dimensions, *Phys. Rev. Lett.* **47**, 882 (1981).
- [42] T. Ando, Quantum point contacts in magnetic fields, *Phys. Rev. B* **44**, 8017 (1991).
- [43] M. Sato, Y. Tanaka, K. Yada, and T. Yokoyama, Topology of Andreev bound states with flat dispersion, *Phys. Rev. B* **83**, 224511 (2011).
- [44] V. Mishra, Y. Li, F.-C. Zhang, and S. Kirchner, Effects of spin-orbit coupling in superconducting proximity devices: Application to CoSi₂/TiSi₂ heterostructures, *Phys. Rev. B* **103**, 184505 (2021).
- [45] V. Mishra, Y. Li, F.-C. Zhang, and S. Kirchner, Effects of spin-orbit coupling on proximity-induced superconductivity, *Phys. Rev. B* **107**, 184505 (2023).
- [46] J. Lee, S. Ikegaya, and Y. Asano, Data used in the figures, https://github.com/ikegayas/data_2501.17369.